

FEM techniques for the LCR reformulation of viscoelastic flow problems

A. Ouazzi, H. Damanik, J. Hron, and S. Turek

Abstract We present special numerical techniques for viscoelastic fluid flow utilizing a fully coupled monolithic multigrid finite element approach with consistent edge-oriented stabilization technique. The governing equations arise from the Navier-Stokes for the Oldroyd-B type of fluid with the help of the log-conformation reformulation to allow a wide range of Weissenberg numbers. The resulting nonlinear system consists of 6 variables for velocity, pressure and the logarithm of the conformation stress tensor in 2D. The system is discretized in time by using a fully implicit second order accurate time integrator. In each time step, we have to solve a discretized system in space employing the high order finite element triple $Q_2/P_1^{disc}/Q_2$. We utilize the discrete damped Newton method with divided differences for handling the Jacobian, and apply a geometrical multigrid solver with a special Vanka smoother to handle the linear subproblems. Local refinement can be assigned at regions of interest to reduce the computational cost. The presented methodology is implemented on the open source software package FEATFLOW (www.featflow.de) and validated for several well-known benchmark problems.

Key words: Viscoelastic flow, LCR reformulation, Edge-Oriented stabilization, Finite Element Method, Newton method, multigrid solver

1 Introduction

The numerical simulation of polymer processing problems incorporates the most important characteristics of viscoelastic fluids. Various nonlinear differential models exist to describe their behavior, but all represent the same numerical challenges, namely the strong coupling between the velocity gradient and the elastic stress which leads to a restriction for the choice of FEM approximation spaces, besides

A. Ouazzi

Institute for Applied Mathematics, TU Dortmund, D-44227 Dortmund, Germany
e-mail: Abderrahim.Ouazzi@math.tu-dortmund.de

H. Damanik

Institute for Applied Mathematics, TU Dortmund, D-44227 Dortmund, Germany
e-mail: Hogenrich.Damanik@math.tu-dortmund.de

J. Hron

Institute of Mathematics, Charles University, Czech Republic
e-mail: hron@karlin.mff.cuni.cz

S. Turek

Institute for Applied Mathematics, TU Dortmund, D-44227 Dortmund, Germany
e-mail: Stefan.Turek@featflow.de

their hyperbolic nature which makes the numerical solution difficult. In this paper, we restrict to the Oldroyd-B model, for testing the monolithic FEM approach [5].

For the Oldroyd-B model [4], the computational rheologist introduces the conformation tensor, which has the special property to be positive definite:

$$\boldsymbol{\sigma}^c = \frac{\eta_p}{\text{We}} (\boldsymbol{\sigma}^p - \mathbf{1}) \quad (1)$$

It is worth to note that this tensor has an integral form with exponential expression

$$\boldsymbol{\sigma}^c(t) = \int_{-\infty}^t \frac{1}{\text{We}} \exp\left(\frac{-(t-s)}{\text{We}}\right) F(s,t) F(s,t)^T ds \quad (2)$$

where $F(s,t)$ is the relative deformation gradient. Then, the set of full equations can be written as

$$\begin{cases} \rho \left(\frac{\partial}{\partial t} + u \cdot \nabla \right) u - \text{div}(2\eta_s \mathbf{D}(u)) + \nabla p + \frac{\eta_p}{\text{We}} \text{div} \boldsymbol{\sigma}^c = 0, \\ \text{div} u = 0, \\ \left(\frac{\partial}{\partial t} + u \cdot \nabla \right) \boldsymbol{\sigma}^c - \nabla u \boldsymbol{\sigma}^c - \boldsymbol{\sigma}^c (\nabla u)^T + \frac{1}{\text{We}} (\boldsymbol{\sigma}^c - \mathbf{1}) = 0 \end{cases} \quad (3)$$

where η_s and η_p are the amount of solvent and polymer contributions respectively. In [6] it is shown for 1D problems that the convection part is not able to balance the exponential growth of the stress. By introducing a new logarithmic variable, the positivity property of the conformation tensor is preserved by design. Indeed the conformation tensor is replaced by its logarithm through exact evaluation, i.e. eigenvalue computations, which leads to the **Log Conformation Representation (LCR)** formulation:

$$\boldsymbol{\psi} = R \begin{pmatrix} \log \lambda_1 & 0 \\ 0 & \log \lambda_2 \end{pmatrix} R^T \quad (4)$$

Here, $\lambda_{i=1,2}$ are the eigenvalues of the conformation tensor $\boldsymbol{\sigma}^c$ and R is the corresponding eigenvector matrix. Then, a new decomposition of the velocity gradient is introduced [4, 6],

$$\nabla u = \mathbf{G} + \boldsymbol{\Omega} + \mathbf{N}(\boldsymbol{\sigma}^c)^{-1} \quad (5)$$

where \mathbf{G} is a symmetric matrix which commutes with the conformation tensor, $\boldsymbol{\Omega}$ is a pure rotation matrix (anti-symmetric matrix) and \mathbf{N} is an antisymmetric matrix. Then, the constitutive laws in terms of conformation tensor $\boldsymbol{\sigma}^c$ and in terms of the log conformation tensor $\boldsymbol{\psi} = \log \boldsymbol{\sigma}^c$ transform respectively into

$$\left(\frac{\partial}{\partial t} + u \cdot \nabla \right) \boldsymbol{\sigma}^c - (\boldsymbol{\Omega} \boldsymbol{\sigma}^c - \boldsymbol{\sigma}^c \boldsymbol{\Omega}) - 2\mathbf{G} \boldsymbol{\sigma}^c = \frac{1}{\text{We}} (\mathbf{1} - \boldsymbol{\sigma}^c), \quad (6)$$

and consequently with $\boldsymbol{\sigma}^c = e^{\boldsymbol{\psi}}$:

$$\left(\frac{\partial}{\partial t} + u \cdot \nabla \right) \boldsymbol{\psi} - (\boldsymbol{\Omega} \boldsymbol{\psi} - \boldsymbol{\psi} \boldsymbol{\Omega}) - 2\mathbf{G} = \frac{1}{\text{We}} (e^{-\boldsymbol{\psi}} - \mathbf{1}) \quad (7)$$

Hence, the new set of equations of the LCR reformulation is written as follows:

$$\begin{cases} \rho \left(\frac{\partial}{\partial t} + u \cdot \nabla \right) u = -\nabla p + \operatorname{div}(2\eta_s \mathbf{D}(u)) + \frac{\eta_p}{\operatorname{We}} \operatorname{div} e^\psi, \\ \operatorname{div} u = 0, \\ \left(\frac{\partial}{\partial t} + u \cdot \nabla \right) \psi - (\boldsymbol{\Omega} \psi - \psi \boldsymbol{\Omega}) - 2\mathbf{G} = \frac{1}{\operatorname{We}} (e^{-\psi} - \mathbf{I}) \end{cases} \quad (8)$$

2 Spatial and time discretization

We apply implicit 2nd order time stepping methods to preserve the high accuracy and robustness in nonstationary flow simulations, for instance the Crank-Nicolson or Fractional-Step- ϑ scheme, which allow adaptive time stepping due to accuracy reasons only, but which do not depend on CFL-like restrictions. Then, the LCR equations are discretized in time as follows:

$$\begin{aligned} & \frac{u^{n+1} - u^n}{\Delta t} + \vartheta \left[\rho u^{n+1} \cdot \nabla u + \nabla p^{n+1} + 2\nabla(\eta_s \mathbf{D}(u^{n+1})) + \frac{\eta_p}{\operatorname{We}} \operatorname{div} e^{\psi^{n+1}} \right] \\ & + (1 - \vartheta) \left[\rho u^n \cdot \nabla u + \nabla p^n + 2\nabla(\eta_s \mathbf{D}(u^n)) + \frac{\eta_p}{\operatorname{We}} \operatorname{div} e^{\psi^n} \right] = 0 \\ & \operatorname{div} u^{n+1} = 0 \\ & \frac{\psi^{n+1} - \psi^n}{\Delta t} + \vartheta \left[u^{n+1} \cdot \nabla \psi^{n+1} - (\boldsymbol{\Omega}(u^{n+1}) \psi^{n+1} - \psi^{n+1} \boldsymbol{\Omega}(u^{n+1})) - 2\mathbf{G}(u^{n+1}) \right] \\ & + (1 - \vartheta) \left[u^n \cdot \nabla \psi^n - (\boldsymbol{\Omega}(u^n) \psi^n - \psi^n \boldsymbol{\Omega}(u^n)) - 2\mathbf{G}(u^n) \right] \\ & - \frac{\vartheta}{\operatorname{We}} \left[e^{-\psi^{n+1}} - \mathbf{I} \right] - \frac{1 - \vartheta}{\operatorname{We}} \left[e^{-\psi^n} - \mathbf{I} \right] = 0 \end{aligned} \quad (9)$$

For the FEM approximation, we utilize the high order $Q_2/P_1^{disc}/Q_2$ finite element triple for discretization in space which can be applied on general meshes together with local grid refinement strategies including hanging nodes. Due to the velocity and stress coupling the choice of the velocity finite element space and the stress finite element space is subject to the LBB condition. In order to use the same finite element space for velocity as well as for the stress one has to use some stabilization techniques. Indeed, to maintain the elliptic character of the momentum equation, the jump term of the following form can be introduced [3, 7]

$$J_u(u, v) = \sum_{\text{edge } E} \max(\gamma_u \eta_p h_E, \gamma_u^* h_E^2) \int_E [\nabla u] : [\nabla v] ds \quad (10)$$

which relaxes the choice of the stress space even in the absence of the pure viscous contribution. Nevertheless the hyperbolic nature of the constitutive equations may require further treatment, so that similarly further jump terms for the stress may be introduced [3]:

$$J_\psi(\Psi, \tau) = \sum_{\text{edge } E} \gamma_\psi h_E^2 \int_E [\nabla \Psi] : [\nabla \tau] ds \quad (11)$$

Then, the discrete system reads as follows

$$\begin{pmatrix} S_u(u) & C & B \\ \tilde{C}^T & S_\psi(u) & 0 \\ B^T & 0 & 0 \end{pmatrix} \begin{pmatrix} u \\ \psi \\ p \end{pmatrix} = \begin{pmatrix} \text{rhs}_u \\ \text{rhs}_\psi \\ \text{rhs}_p \end{pmatrix} \quad (12)$$

where $S_u = \frac{1}{\Delta t} M_u + L_u + K_u + J_u$, $S_\psi = \frac{1}{\Delta t} M_\psi + K_u + K_\Omega + J_\psi$, M_u and M_ψ are mass matrices, L_u is the discrete diffusion operator, K_u the discrete convective term, K_Ω is the discrete operator such that $K_\Omega \psi = -(\Omega \psi - \psi \Omega)$, $\tilde{C}^T = M_{\mathbf{G}(\nabla u, \sigma^c)}$, and C is the discrete matrix of $-\frac{\eta_p}{\text{We}} \nabla \cdot \exp$. Furthermore, B and B^T are discrete analogues to the gradient and divergence operators.

3 Nonlinear and linear solvers

The strongly coupled system (12) is then linearized through a discrete Newton approach which results in the solution steps of the form

$$x^{n+1} = x^n + \omega^n J(x^n)^{-1} R(x^n)$$

where ω^n is a damping parameter. In this approach, we approximate the Jacobian $J = \left[\frac{\partial R(x^n)}{\partial x} \right]$ using divided differences

$$\left[\frac{\partial R(x^n)}{\partial x} \right]_{ij} \approx \frac{R_i(x^n + \varepsilon e_j) - R_i(x^n - \varepsilon e_j)}{2\varepsilon} \quad (13)$$

with $x = (u, \psi, p)$, $R(x)$ is the residual coming from the discrete problem of the system (12), and $e_i = \delta_{ij}$ is the standard Kronecker symbol. Hence, the resulting linear system is a typical saddle point problem which is solved effectively using coupled multigrid [4, 5], i.e. local Pressure Schur Complement approach as generalization of so-called Vanka smoothers which are simple iterative relaxation methods for such coupled systems of saddle point type. The smoothers are acting directly on element level and are embedded into an outer block Jacobi/Gauss-Seidel iteration. The local character of this procedure together with a global defect-correction mechanism is crucial for this monolithic approach:

$$\begin{bmatrix} u^{n+1} \\ \psi^{n+1} \\ p^{n+1} \end{bmatrix} = \begin{bmatrix} u^n \\ \psi^n \\ p^n \end{bmatrix} + \omega^n \sum_{T \in \mathcal{T}_h} J|_T^{-1} \begin{bmatrix} R_u \\ R_\psi \\ R_p \end{bmatrix} |_T \quad (14)$$

The coarse grid discretizations are effectively done using the finite element approach, and the grid transfer operators (restriction and prolongation) are standard due to the conforming approximation. Here, the 'summation' over each element $T \in \mathcal{T}_h$ represents an assembling technique.

4 Numerical examples

For prototypical numerical tests of this new approach, we consider the numerical simulation of both directly steady and nonstationary flow in a lid-driven cavity for the Oldroyd-B model. The initial condition for the stress tensor is unity and a regularized velocity boundary condition is implemented such that $u(x, t) = (8(1 + \tanh 8(t - 0.5))x^2(1 - x)^2, 0)^T$ on the top boundary while zero velocity on the rest of boundary is prescribed. For direct steady simulations the velocity profile evolves to $u(x, t) = (16x^2(1 - x)^2, 0)^T$ on the boundary. For the total viscosity (zero-shear viscosity), η_s and η_p are equal to 1. The simulation is performed with the mesh size $h = 1/64$ and with coarse mesh size $h = 1/4$. The time step is chosen to be $\Delta t = 0.1$ in the sense that no further improvement in kinetic energy with respect to smaller time steps could be observed. The number of cells for the corresponding computation level n is $Ln = 2^{4+2n}$. We calculate the kinetic energy by $\frac{1}{2} \|u_h\|_{L_2(\Omega)}^2$ and analyze the impact of jump stabilization for different We numbers. For $We=1$,

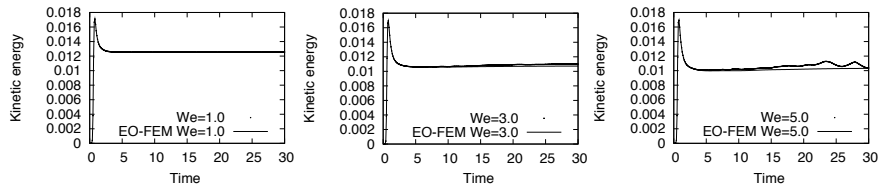


Fig. 1 Driven cavity flow: Kinetic energy until $t = 30$ for different We numbers with and without EO-FEM.

the kinetic energy seems to reach a steady state as shown in Fig. 1 and it remains steady at least up to time $t = 30$. As the We number increases the kinetic energy oscillates stronger and the LCR variable becomes more spurious at time $t = 30$, see Fig. 2. Longer computation times may lead to numerical break down. EO-FEM in this case is able to relax these oscillations, thus it significantly improves numerical stability.

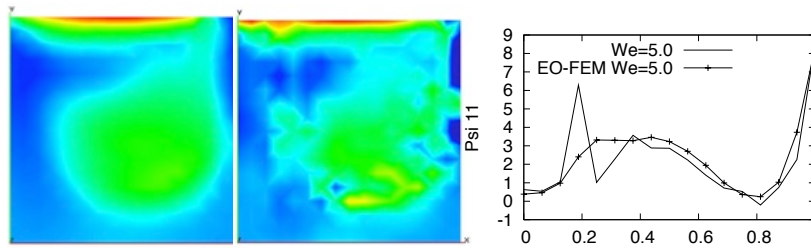


Fig. 2 Driven cavity flow: The plot of the stress ψ_{11} with EO-FEM (left), without EO-FEM (middle) and the Cutline of ψ_{11} at $x = 0.5, t = 30$ with and without EO-FEM (right).

Next, we consider planar flow around cylinder and plot the drag up to $We = 1.8$ in which the drag coefficients are comparable with other authors as can be seen in Fig. 3. However, it is remarkable that with the LCR formulation, results for quite high Weissenberg numbers in comparison to standard formulation can be easily obtained. While usually the maximum We number, which can be obtained by LCR,

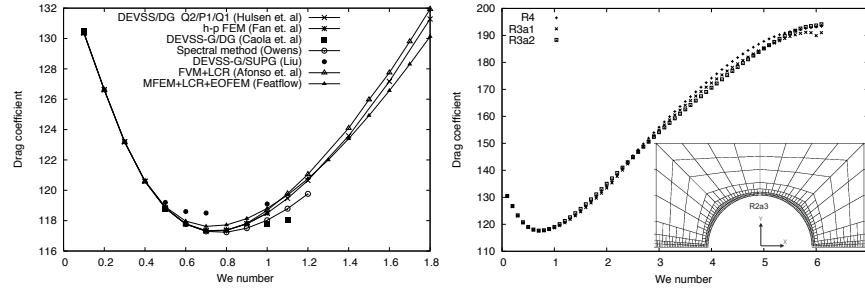


Fig. 3 Planar flow around cylinder: Drag coefficient from different authors (left) and for different levels for higher We with EO-FEM (right) and one exemplary computational mesh with local refinement.

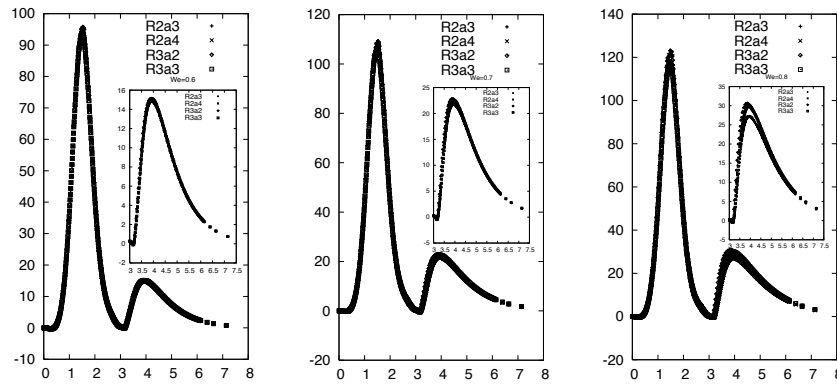


Fig. 4 Planar flow around cylinder: Normal stress convergence with local refinement for Weissenberg numbers $We = 0.6$ (left), $We = 0.7$ (middle) and $We = 0.8$ (right) with the zoom of in the wake part.

is in the range of $We = 1.8$ or $We = 2.0$, see [1, 6], here EO-FEM helps to go further as far as $We = 6.0$. Note that this is calculated with a direct steady approach which shows the big potential of EO-FEM for viscoelastic flow. Further results can be seen in Fig. 4 where for all three We numbers the stress converges for four different meshes except for $We = 0.8$ a small difference in the wake between two regular refinements. As mentioned before, the linear subproblem is handled by a special monolithic multigrid solver. In Table 1 we show the corresponding convergence behavior in a direct steady approach with respect to the number of nonlinear iterations for increasing We numbers. Multigrid seems to be stable with respect to the mesh refinement and the nonlinearity of the problem as the number increases.

Table 1 Newton-multigrid behaviour: Nonlinear iterations (NNL)/Average multigrid sweeps (AVMG) per nonlinear iterations for several levels refinement (Ri, $i=1,4$), different We numbers and different linear tolerance parameters ε for planar flow around cylinder configuration.

We	0.01		0.1		1.0	
ε	0.1	0.01	0.1	0.01	0.1	0.01
R1	9/2	5/3	10/1	7/3	14/1	10/3
R2	9/3	5/5	10/2	7/4	16/2	10/5
R3	9/3	5/6	10/3	7/5	16/2	11/5
R4	9/3	5/6	10/3	9/5	13/3	11/5

Finally, we present preliminary results for the planar 4:1 contraction problem which is one of the most well-known benchmarks for viscoelastic flow. As a current result for this configuration, we are able to reproduce the qualitative phenomenon of lip vortex growth with respect to increasing We number (Fig. 5) in which case we perform the calculations on a locally refined mesh with hanging nodes as shown in Fig. 6.

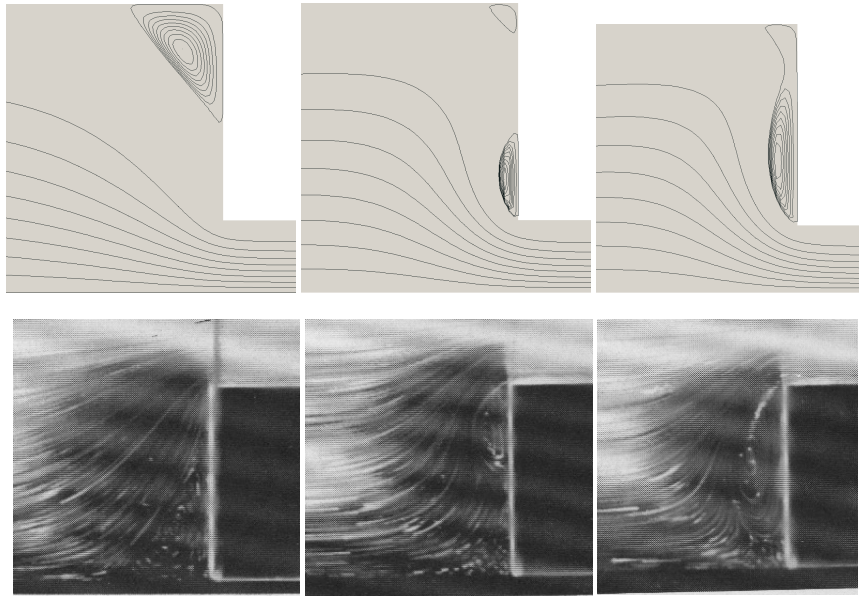


Fig. 5 Lip vortex growth for Oldroyd-B model: Numerical simulation (top) versus experiment (bottom [2]) for lip vortex growth in a 4 to 1 contraction.



Fig. 6 The planar 4:1 contraction: Computational mesh with local refinement.

5 Conclusion

We have presented special numerical simulation techniques for viscoelastic flow within a monolithic finite element framework of utilizing the new LCR technique for Oldroyd-B type of fluids. Edge-oriented FEM stabilization is implemented to increase the numerical stability. Together with local refinement the method shows to be a very promising way for solving viscoelastic flow problems particularly for high We numbers. Several numerical examples of cavity flow, flow around cylinder and the growth of lip vortex in a contraction flow are also presented. Numerical stability has been significantly improved by the help of stabilization and mesh convergence for the stress variable can be achieved for several Weissenberg numbers in the flow around cylinder configuration. Future work will include the implementation of LCR in other viscoelastic models together with an additional coupling of the energy equation with a viscous dissipation term, see [5], in order to be able to simulate more realistic flow problems, particularly in 3D.

Acknowledgements This work was supported by the German Research Association (DFG) through the collaborative research center SFB/TRR 30 and through the grants TU 102/21 and by the Graduate School of Production Engineering and Logistics.

References

- [1] Afonso, A., Oliveira, P.J., Pinho, F.T., and Alves, M.A. The log-conformation tensor approach in the finite-volume method framework. *J. Non-Newt. Fluid Mech.*, 157:55–65, 2009.
- [2] Boger, D. V. and Walters, K. *Rheological Phenomena in Focus*. Elsevier, 1993. Amsterdam.
- [3] Bonito, A. and Burman, E. A continuous interior penalty method for viscoelastic flows. *SIAM Journal of Scientific Computing*, 30:1156–1177, 2008.
- [4] Damanik, H., Hron, J., Ouazzi, A., and Turek, S. Finite element discretization and Newton–multigrid solution techniques for the log–conformation reformulation (LCR) of viscoelastic flow problems. *J. Non-Newt. Fluid Mech.*, 2009. submitted.
- [5] Damanik, H., Hron, J., Ouazzi, A., and Turek, S. A monolithic FEM–multigrid solver for non–isothermal incompressible flow on general meshes. *Journal of Computational Physics*, 228:3869–3881, 2009.
- [6] Hulsen, M. A., Fattal, R., and Kupferman, R. Flow of viscoelastic fluids past a cylinder at high weissenberg number: Stabilized simulations using matrix logarithms. *J. Non-Newt. Fluid Mech.*, 127:27–39, 2005.
- [7] Turek, S. and Ouazzi, A. Unified edge–oriented stabilization of nonconforming FEM for incompressible flow problems: Numerical investigations. *J. Numer. Math.*, 15:299–322, 2007.